Design and Construction of an Affordable Phantom for Electron Density Measurement and Linearity Tests of Computed Tomography Systems

Rezvan Ravanfar Haghighi[1*], Sabysachi Chatterjee[2], Sepide Sefidbakht[1], Reza Jalli[1], Vardhan Chatterjee Vani[3]

1. Medical Imaging Research Centre, Shiraz University of Medical Sciences, Shiraz, Iran
2. Ongil, 79 D3, Sivaya Nagar, Reddiyur Alagapuram, Salem 636004. India
3. Department of Instrumentation and Applied Physics, Indian Institute of Science, India, Bangalore

A R T I C L E I N F O	A B S T R A C T
	Introduction: The performance of computed tomography is routinely checked using phantoms, which are known as important diagnostic imaging tools. Depending upon the aim of the study, different phantoms are designed, while trying to satisfy certain levels of diversities in their application. ***Material and Methods:*** The present study describes the construction of an inexpensive phantom designed for simultaneous measurements of 12 different samples. The body of the phantom, test tube holders, and test tubes were made of materials of low attenuation coefficient. Body of the phantom was filled with water. Test tubes filled with solutions of known chemical compositions were mounted on the test tube holders. The whole phantom was scanned at 80, 100, 120, 140 kVp to evaluate the performance of the CT system. Using Hounsfield Unit (HU) data from these liquid samples of known electron density, the phantom was calibrated for electron density measurements. ***Results:*** The system's accuracy and reproducibility were verified by measuring the HU values for some known materials. According to the results obtained from the experimental data with liquid samples, the accuracy of the water and noise was within ±3.2 HU and 0.6%, respectively. Moreover, the image uniformity error was less than ±2 HU, and CT system's linearity for calibration was estimated with 99.9% confidence. ***Conclusion:*** The present system gives satisfactory results with known samples and can be used with confidence for characterizing unknown materials.

Introduction

Computed tomography (CT) is probably the most commonly used non-invasive diagnostic tool in imaging the armamentarium with the superb spatial and temporal resolution, detection, and characterization of various structures in the human body [1,2]. A quantitative study by CT system helps the physician to characterize normal and abnormal tissues. Several quantitative studies involve mineral content measurement in bones, tissue characterization by dual-energy CT, histogram analysis, and dose distribution calculations utilizing the calibration curve of electron density versus Hounsfield Unit (HU) value for treatment planning in radiotherapy [3-5].

In order to use the CT system for quantitative study, the performance of CT machine should be evaluated to produce reliable HU values. Moreover, the ability of CT system should be assessed to measure a broad range of HU values, such as air, fat tissue, soft tissue, and bone following the tests that are explained in detail in credible sources, such as International Atomic Energy Agency IAEA publications [6-8].

It is well known that the basis of the CT images is the attenuation coefficients of the materials along the x-ray beam path that are normalized with respect to the attenuation coefficient of water. Therefore, at any specified excitation voltage (V), the HU value is defined using the following *Equation* [9]:

$$HU(V) = \frac{\hat{\mu}(V) - \hat{\mu}_w(V)}{\hat{\mu}_w(V)} \times 1000 \qquad (1)$$

Where, $\hat{\mu}(V)$ and $\hat{\mu}_w(V)$ are the mean linear attenuation coefficients of the sample and water respectively. They are calculated over the entire source spectrum and taking X-ray detector efficiency into account for different energies of the source spectrum.

Corresponding Author: Tel: +98 7136281464; Fax: +98 7136281506; E-mail: sravanfarr@gmail.com

According to *Equation* (1), the HU values of water and air are equal to zero and -1000, respectively. The reliability of the CT is checked by ascertaining if at any specified excitation voltage (kVp), the HU value for water lies within *±4*, which is the standard acceptable range [9-11]. This can be tested simply by scanning water filled in a plastic container.

The deviation of the HU values between the pixels inside the selected areas of a homogeneous material, such as water is related to the standard deviation arising out of the noise in the system due to the statistical nature of the X-ray production. In addition, noise is contributed by the interaction of the X-ray photon with the subjects on the path of the x-ray beam. Noise degrades image quality and is an impediment to adequate interrogation of low contrast subjects on the CT image. Furthermore, it creates difficulties to recognize and select the proper location of a lesion on the CT image. It is necessary that quantitative studies utilize CT system to test the reliability and accuracy of the HU values over a broad range. Regarding the importance of noise estimation, the acceptable range of standard deviation for noise is 25% of the baseline value [7-11].

The visual assessment of the CT slice of the uniform phantom, such as water is a very useful tool to evaluate the presence of the image artifacts. Streaking, ring, shading and aliasing artifacts may interfere with the diagnostic ability of CT images. Image artifacts can be detected using scanning axial slices in a water phantom. Moreover, it can evaluate the uniformity of the images. The HU values of a uniform material, such as water should be the same or close to each other across the slice of CT image of the water or any other homogeneous material in the phantom. It is important to note that the variation of the HU values due to beam hardening effect from the periphery to the center of the water phantom should be corrected properly by a suitable algorithm.

This test is necessary for quantitative studies that make use of CT machines. The maximum variation between the HU values at different locations of the homogeneous material, such as water should be within ±4 in order to be acceptable for image uniformity [7, 9-11].

The other requirement concerns the ability of the CT system to accurately detect a wide range of HU values of normal and abnormal tissues with different types of effective atomic numbers (Z_{eff}) and physical density (ρ) at different tube voltages. Regarding the accurate measurement of the attenuation coefficient for most types of normal and abnormal tissues, it is necessary to test the linearity of the CT system. The linearity of the CT machine is recognized as an important issue since the early days of CT invention. The problem is lack of no proper test tool to evaluate the linearity of the CT system. As Kalender stated. [10], different types of plastic materials, which are used in the present-day phantoms do not have a proper specification for the linearity tests. In the present study, this will be a major concern and a method is presented that has the potential to be accepted as a standard.

There are large numbers of commercial phantoms available in the market to control quality of the CT scanners. In addition, these custom-made devices are made by research groups to satisfy the requirements of high accuracy and low price in diagnostic energy range, and record images simultaneously from a large number of samples [12, 13]. These phantoms are useful to test the performance of the CT machine in order to be sure about the quantitative reliability. The standard commercial phantoms manufactured by the imaging industries in a handful of developed countries are marketed at prohibitive prices at times beyond the reach of most laboratories and hospitals in the developing countries.

This acted as a "guiding idea" to design and construct a simple and inexpensive phantom which is able to perform the most essential quality control tests, such as check the accuracy of HU value, record noise measurement, image uniformity, and image artifacts with a further aim to test the linearity of CT machines.

Moreover, this simple phantom can be reliably used in quantitative studies, such as electron density measurement for radiotherapy proposes and the calibration of the CT machine for the inversion of dual energy computed tomography (DECT) data [14] utilizing the algorithm developed in this study.

Materials and Methods

The phantom was designed for essential quality control tests of the CT system, especially for linearity test of CT machine and electron density measurement. It consists of two parts, including the permanent body of the phantom and replaceable test-tubes. Body of the phantom is a cylinder, with a circular cross-section containing test tube holders. The diameter and length of the phantom are 20 cm and 17 cm, respectively, as shown in Figures 1.a and b.

With these dimensions, it was possible to fit 12 test tubes in the phantom with sufficient water surrounding them, thereby providing an adequate and compact system for quality control studies, beam hardening studies, linearity test, and data collection for the development of DECT inversion algorithm.
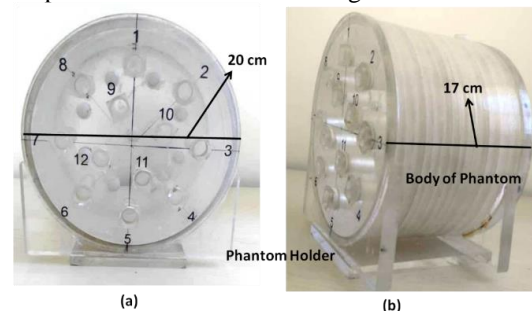

Figure 1. Front view of the body of the phantom with 20 cm diameter (a) and its lateral view with 17 cm length (b).

The phantom is made of Plexiglas and is filled with distilled water. Test tube holders are made of Polymethyl methacrylate and are drilled mounted in two rows in which 8 and 4 tube holders are in the outer and inner rows, respectively, being inserted through holes that are drilled on the upper lid of the phantom (Figures 1.a and 1.b). Test tube holders and the test tubes are surrounded by water within the body of the phantom. The outer and inner rows of test tube holders are located at depths of 2.5 cm and 5.0 cm, respectively, from the surface of the phantom. The separation angle is 45° and 90° between test tube holders at the outer and inner layers, respectively. Each test tube holder has 1.5 cm inner diameter and is 10 cm in length. They are held perpendicular to the scanning plane parallel to the z-axis of the scanner table. The aim of designing the phantom with two rows of the test tube holders at different depths of water as measured from the outer wall of the phantom was to assess the beam hardening effect at different depths of the water phantom.

Every test tube can hold up to 17 ml of material, and the phantom weighs about 5.50 kg when completely filled. It is not too heavy and fairly compact for hospital staff to handle for routine tests of CT machines and to be conducted from time to time. This is the main purpose that the phantom was designed for while keeping cost affordability in mind.

In the construction stage and during mechanical testing, no leakage was detected from the phantom. This was also checked by filling the system with water and checking the system from time to time for 168 hours (one week). Special care was taken to check the joints in the system and all were confirmed to be leak proof.
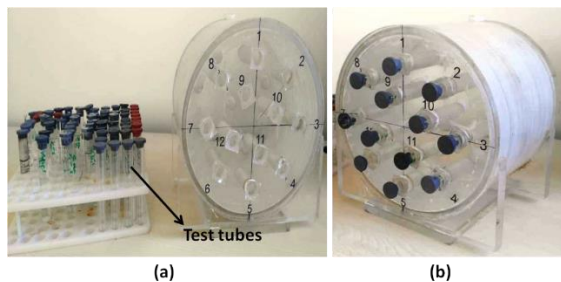

Figure 2. Test tubes filled up with water or chemical solutions (a) and inserted into the test tube holders (b).

The test tubes in Figure 2.a are made of plastic material with a very low X-ray attenuation coefficient. These can be procured from any laboratory equipment supplier. These selected test-tubes have 1.45 cm inner diameter and 10 cm in length. Test tubes containing pure water or chemical compounds are inserted into the test tube holders, which are surrounded by water as is shown in Figure 2.b.

The body of the phantom is attached to the kickstand or phantom holder, which is made of Plexiglas (Figure 1). Kickstand of the phantom fixes the body of the phantom in its correct position on the scanner table during quality control tests.

Chemical compounds were selected on the basis of their availability, generally available in any simple chemistry lab. Moreover, a large range of values of effective atomic number (Z_{eff}) and electron density (ρ_e) was taken into account when selecting the compound. Aqueous solutions of different chemicals were made and their weight/weight (w/w %) concentrations were noted. Choices were made so that one got solutions with different known electron densities with low, medium, and high effective atomic numbers.

These aqueous solutions of methanol, glycerol, and potassium hydroxide (KOH) were made with 8 different concentrations with their Z_{eff} values matching those of low, medium, and high Z_{eff} tissues such as fat, soft tissue, as well as muscle and spongy bone, respectively.

The aforementioned chemical compounds were purchased from Merck Company. For low Z_{eff} substances, such as methanol and glycerol, the solutions at concentrations of 5, 10, 15, 20, 25, 30, 35, and 40% in water were very accurately made in the laboratory.

The solution for KOH was saturated with 40% w, and thus the solutions were made at concentrations of 5, 10, 15, 20, 25, 30, and 35%. The weight measurements were made by a balance with 0.001-gram accuracy. Physical density of each solution was determined by the standard method of using specific gravity bottle and compared with the reference values [15, 16] given in the literature.

Liquid systems have been employed for testing and calibration purpose in this study since liquids are more homogeneous. For this reason, such samples are far less prone to errors due to nonlinearity [10, 17]. In view of this uniformity in electron density and the importance of linearity test, liquid mixtures of known electron density (ρ_e) and effective atomic number (Z_{eff}) have always been used for calibration purpose. These two physical quantities of the system, namely, electron density and effective atomic number were calculated from the known compositions of the mixture as were used in sample preparation. These calculations were done according to the formula given in the literature [18, 19], as follows:

Let us consider a mixture of different substances in which molecules of type "j" are present as a fraction $c(j)$ of the total number of molecules. Furthermore, let this j-th type compound have a chemical formula $M(j) = \Sigma n(j,i) A_i$.

Then, the electron density of the mixture in terms of the density ρ of the substance is given by:

$$\rho_e = \left(\frac{\rho}{m_p}\right) \frac{\sum_j c(j) \sum_i n(j,i) z_i}{\sum_j c(j) \sum_i n(j,i) A_i} \qquad (2)$$

where, $m_p = 1.67 \times 10^{-24}$ gm is the proton mass, and A_i and Z_i denote the atomic weight and number of the atom of type "i", respectively. The quantity Z_{eff}^x, which pertains to the photoelectric effect is given by:

$$Z_{eff}^x = \frac{\sum_j c(j) \sum_i n(j,i) z_i^{x(t)+1}}{\sum_j c(j) \sum_i n(j,i) z_i} \qquad (3)$$

Where, x (i) is the exponent of photoelectric effect for atom "i".

Choosing any arbitrary p>0, the effective atomic number is defined as follows:

$$Z_{eff} = \left[\frac{\sum_j c(j) \sum_i n(j,i) z_i^{p+1}}{\sum_j c(j) \sum_i n(j,i) z_i} \right]^{1/p} \qquad (4)$$

It is to be noted that while ρ_e and Z_{eff}^x are quantities natural to the substance, Z_{eff} is not natural; however, it is decided by the choice of *p*. The photoelectric indices *x(i)* are not constant for different types of atoms, except that it is known to be x=4 for the case of the hydrogen-like atom, as obtained from basic theory. For other atoms, it is known that *x(i)* lies within a range of 3.0-4.0. In the present study, the Z_{eff} is calculated by choosing p=4, and x=4 was utilized for all atoms [18, 19].

Considering these definitions, we obtain:

$$\hat{\mu}(V) = \rho_e \left[\alpha(V) + \beta(V) Z_{eff}^x \right] \qquad (5)$$

where, $\hat{\mu}(V)$ and $\hat{\mu_w}(V)$ are the average attenuation coefficients of the substance and water, respectively, while *α (V)* and *β (V)* represent the average coefficients of Compton effect, and the photoelectric effect where the averages are taken over the source spectrum of the CT system and the detector response.

Furthermore, a quantity F (V) is defined as follows:

$$F(V) \equiv 1 + \frac{HU(V)}{1000} = \frac{\hat{\mu}(V)}{\hat{\mu}_w(V)} \qquad (6)$$

Considering *Equations* (5, 6), we obtain:

$$\frac{F(V)}{\rho_e} = a(V) + b(V) Z_{eff}^x \qquad (7)$$

where, $a(V) = \alpha(V)/\hat{\mu}_w(V)$ and $b(V) = \beta(V)/\hat{\mu}_w(V)$. Conversely, if the ρ_e and Z_{eff}^x of the substance are known, its HU (V) value can be predicted using *Equations* (6,7) as follows:

$$HU(V) = -1000 \times \left[1 - \{a(V) + b(V) Z_{eff}^x\} \rho_e \right] \qquad (8)$$

This can be approximated as:

HU(V)≈-1000×(1-{a(V)+3277×b(V)}(ρₑ(water)/ρ(water))ρ)   (9)

For substances whose $Z_{eff}^x \approx 3277$(i.e., close to that of water), their electron density can also be approximated as $\rho_e \approx$ (ρ_e(water)/ ρ(water)) ρ).

For any observation, the recorded HU (V) value may have statistical fluctuations δHU (V) implying corresponding variations in $\hat{\mu}(V)$; accordingly, F *(V)* fluctuates by δF(V), as are given by, :

$$\delta \hat{\mu}(V) = \hat{\mu}_w(V) \left[\frac{\delta HU(V)}{1000} \right] \qquad (10)$$

$$\delta F(V) = \delta HU(V)/1000 \qquad (11)$$

Therefore, their relative fluctuations are obtained as:

$$\frac{\delta \hat{\mu}(V)}{\hat{\mu}(V)} = \frac{\delta HU(V)/1000}{F(V)} = \frac{\delta F(V)}{F(V)} \qquad (12)$$

Using the recorded data of HU (V) for different samples, least square fit test was performed for *Equation* (6). For low and high Z_{eff} solutions, such as glycerol (known as medium Z_{eff}), and KOH (known as high Z_{eff}), a linear least square fit Y= a + bX was sought in the form.

y= F (V)/ρe, X=Z_{eff}^x, and "*a*" and "*b*" are the coefficients of least square fit. In unknown cases, HU(V) value can be simply measured by scanning the sample, and F(V) values would be calculated from the data using *Equation* (6).

Then, the electron density can be predicted as follows:

$$\rho_e = \frac{F(V)}{a(V) + b(V) z_{eff}^x} \qquad (13)$$

It follows *Equation* (7), and the values of a(V) and b(V) are those found from the least square fit, as described above. Furthermore, for $Z_{eff} \approx Z_{eff}$ *(water)* =3277 as is the case in several human tissues, one can approximate:

$$\rho_e \approx \rho_e' = \frac{F(V)}{[a(V) + 3277 \times b(V)]} \qquad (14)$$

Scanning Parameters

Homogeneous solutions were selected in this study since non-linear effects get pronounced in substances with partial volume effects. The liquid samples were kept in a fridge at 4°C far away from the boiling point of water and were kept isolated from mechanical vibrations and agitations. Accordingly, bubble-nucleation was also prevented due to cavitation. Bubble formation while filling the test tubes was avoided by gently pouring the liquids in the test tubes. Subsequently, it was noted that bubbles did not form due to evaporation or expulsion of dissolved gases.

The phantom was placed on the top of the scanner table in such a way that the long axis of the test tube holders was aligned along the Z-axis and perpendicular to the scanning plane. The GE Health Care (8) Slices MDCT scanner system was used for all image acquisitions. In recording the HU of the samples, measured HU value of each sample was corrected by subtracting the HU value of the corresponding test tube containing water.

Therefore, we obtain:

$$HU_{corrected} = HU_s - HU_w \qquad (15)$$

Where, HU_s and HU_w represent the respective HU values of solution and water in the corresponding test tube. Topogram of the phantom was initially obtained in order to help design the subsequent slices through water

and test tube holders of the phantom. Axial slices were obtained from water and test tubes at 80, 100, 120, 140 kVp with a tube current of 150 mAs, and a H31s convolution kernel with 5 mm slice thickness. The same protocols were used to scan the water and chemical compounds by simply replacing the water-filled test tubes with those filled with methanol, glycerol, and KOH solutions. To test the linearity of the CT machine, each series of chemical compounds was scanned separately by inserting the test tube containing the lowest concentration, (5% w/w) into the position of 12 o'clock of the test tube holder.

The other test tubes containing solutions with w/w concentrations of 10, 15, 20, 25, 30, 35, and 40% were placed at equal intervals on the outer ring of the test tube holders. Since KOH solution saturated at w=40%, the test tube number 8 was filled with water. Similarly, the test tubes containing solutions with 10, 20, 30, 40% w/w were placed in the inner row of the test tube holders. Beam hardening effects can be tested by comparing the HU values in the two rows of test tubes. All axial slice images were saved in a picture archiving and communication system for evaluation.

Axial slice of the water portion of the phantom was scanned at 120 kVp, and was used to assess the accuracy of HU value, image noise, and uniformity test. The HU values of water and chemical compounds with different concentrations (5% to 40% w/w) were measured by selecting the region of interest (ROI), at proper positions inside the axial CT image of the test tubes (Figures. 3.a and 3.b). The ROIs were selected in such a way that they did not contaminate with neighboring structures so that there was no error due to partial volume effect.
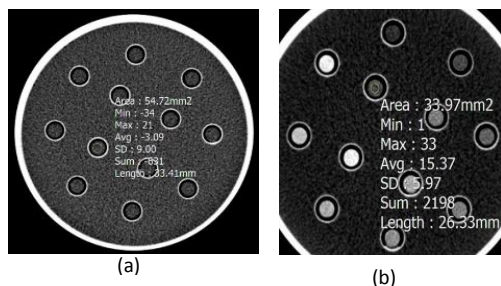

Figure 3. Computed tomography image of test tubes scanned at 120 kVp, containing water (a) and different concentrations of glycerol in the outer layer (5, 10, 15, 20, 25, 30, 35,and 40% w/w) and inner layer (10, 20, 30, and 40% w/w) (b). Circular region of interest inserted inside the test tube without contamination with neighboring structure.

Figure. 4 displays the variation of the $HU_{corrected}$ values versus concentrations for each chemical compound, such as methanol, glycerol, and KOH. This plot evaluates the linearity of the CT machine.

Calibration for Electron Density Measurements

In the next stage, the suitability of the phantom was assessed for the measurement of electron density of the samples. This was based on the determination of the parameters a (V) and b (V), as given in *Equation* (7). This was performed using least square fit with HU (V)

data at V=80,100,120,140 kVp for samples with different ρ_e and Z_{eff}^{x} values.

Results

Table 1 presents the values of X and Y (V) obtained from the data in this study. Plot X was made versus Y (V) plot of different samples placed in the inner and outer test tubes (Figure 5). It can be seen that the data points lie close to each other indicating a very little discrepancy due to beam hardening effect when the X-ray beam travels through water or other material with low and medium attenuation coefficients. In fact, the difference between the inner and outer layers regarding the F (120) values was less than 3%.

Table 1. Records of *X* and *Y* for different solutions of KOH, glycerol, and methanol. The KOH and glycerol data are used to obtain the least square fit of the type given in *Equation* (7).

Sample	(w/w %)	X	Y(80)	Y(100)	Y(120)	Y(140)
	5	7181	0.3228	0.3167	0.3135	0.3115
	10	11125	0.3524	0.3419	0.3355	0.3309
	15	15108	0.3705	0.3546	0.3422	0.3326
	20	19133	0.3972	0.3743	0.3601	0.3512
	25	23198	0.4311	0.4027	0.3841	0.3723
	30	27306	0.4541	0.4180	0.3964	0.3826
KOH	35	31456	0.4734	0.4332	0.4076	0.3923
	5	3236	0.2983	0.2974	0.2971	0.2974
	10	3194	0.2957	0.2960	0.2966	0.2966
	15	3153	0.2973	0.2978	0.2978	0.2978
	20	3111	0.2990	0.2990	0.2996	0.2999
	25	3069	0.2988	0.2994	0.2997	0.3000
	30	3028	0.2992	0.2995	0.3000	0.3000
	35	2986	0.3015	0.3026	0.3023	0.3032
Glycerol	40	2944	0.3002	0.3005	0.3013	0.3019
	5	3225	0.3093	0.3090	0.3087	0.3090
	10	3173	0.3084	0.3091	0.3100	0.3097
	15	3122	0.3082	0.3092	0.3095	0.3095
	20	3070	0.3086	0.3096	0.3099	0.3102
	25	3019	0.3097	0.3100	0.3106	0.3106
	30	2967	0.3108	0.3108	0.3114	0.3117
	35	2916	0.3092	0.3109	0.3112	0.3115
Methanol	40	2864	0.3094	0.3103	0.3113	0.3117

As can be observed from the figure 5, the differences between the outer and inner test tubes in terms of F(120) values containing concentrations at 10, 20, 30, and 40 % of w/w are negligible for methanol, glycerol, and KOH (10, 20, and 30 % of w/w) solutions.

The linearity of the CT machine for different ranges of the HU values is shown in Figures 4.a, 4.b, and 4.c for methanol, glycerol, and KOH, respectively.

For KOH, the w=40% data was not used since the solution was supersaturated for this concentration. The

HU values of the low, medium, and high Z_{eff} chemical solutions with different concentrations from 5 to 40% w/w% (with 5% increment), such as glycerol (low and medium Z_{eff}^{x}) and KOH (high Z_{eff}^{x}) are used to plot the least square fit.
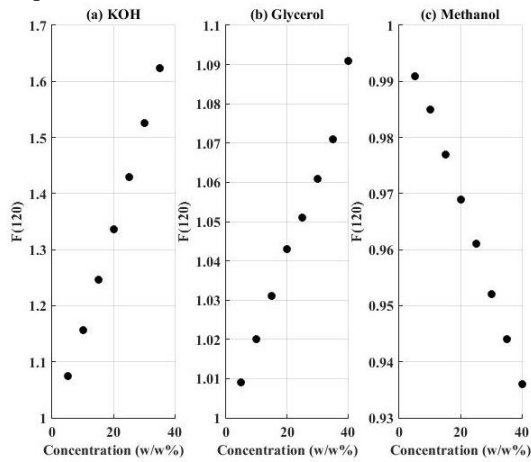

Figure 4. Variation of HU (120) versus different concentrations of (a) (5, 10, 15, 20, 25, 30, 35 w/w %) of potassium hydroxide, (b) and (c)) (5, 10, 15, 20, 25, 30, 35, 40 w/w %) glycerol, and methanol.
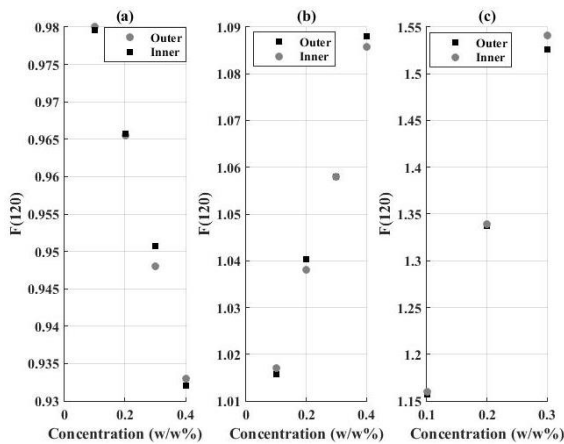

Figure 5. Plot F (120) versus concentration of solutions in w/w% kept in the inner and outer layers of the phantom for (a) methanol, (b) glycerol and (c) potassium hydroxide.

Figure 6 shows a linear fit between the $F(V)/\rho_e$ for 15 data points from glycerol and KOH. The correlation is very close to one shown in Figure 6 (a-d) at 80, 100, 120, and 140 kVp. These least square fits can be used to calculate electron density. Since human body consists of low, medium, and high Z_{eff} (very similar to glycerol and KOH) materials, the coefficients "*a*" and "*b*" (found by least square fit) observed in this case can accurately estimate the electron density of unknown scanned tissues.

The least square fits are found to be very good with a level of confidence greater than 99% (P<0.01, Figure 6). The data in Figure 6 correspond to the cases with *7.3970<Z_{eff}<13.3179* and *3.3962×10^{23} <ρ_e<3.9839×10^{23}*. Such cases abound in soft tissues, such as adipose, muscle, and liver as well as spongy bone which are very

important in diagnostic imaging as well as radiotherapy treatment planning.

The results of the least square fits are shown in Table 2.

Tables 3-5 display the validity of the least square fits and their ability to predict the electron density of substances. It is to be noted that the KOH and glycerol data were used for the calibration purpose by least square regression. The data for methanol is used to predict the ρ_e and $\rho_{e'}$ with a substance that was not used for calibration.
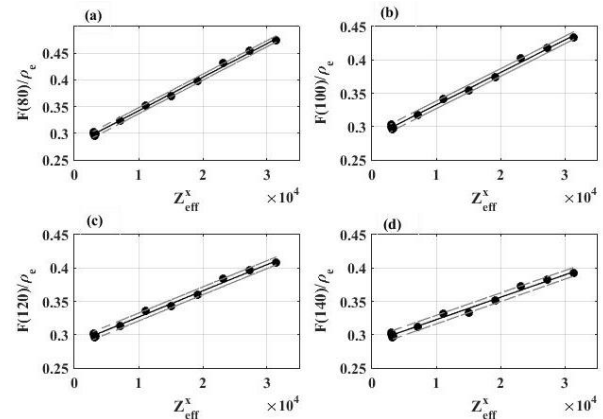

Figure 6. Variation of F (V)/ρ_e, versus Z_{eff}^{x} at 5 to 40% w/w concentration of glycerol and 5-35% KOH. Least square fits are made for 15 data points (most of the glycerol data are clustered between 2900 <Z_{eff}^{x} < 3200 and are thus not distinguishable) at (a) 80 kVp with a=0.2792±0.008, b=(6.2995×10^{-6})±(8.3×10^{-8}), r^2=0.9978, (b) 100 kVp with a=0.2841±0.008, b=(4.539×10^{-6})±(8.26×10^{-8}), r^2=0.9962, (c) 120 kVp with a=0.2872, b=(3.935×10^{-6})±(8.56×10^{-8}), r^2=0.9962, and (d) 140 kVp with a=0.2891, b=(3.355×10^{-6})±(9.36×10^{-8}), r^2=0.9939 .

Table 2. Coefficients a (V) and b (V) obtained from the least square fit with *Equation* (7) of potassium hydroxide and glycerol data as are given in Table 1.

kVp	a(V)	b(V)×10^{-5}	r^2	p
80	0.2792	0.6300	0.9978	< 0.01
100	0.2841	0.4854	0.9962	< 0.01
120	0.2872	0.3935	0.9939	< 0.01
140	0.2891	0.3355	0.9900	< 0.01

According to the compared results of electron density calculation obtained from *Equations* (13) and (14) (Tables 3-5), the parameters *a* (V) and *b* (V) are obtained from calibration experiments.

It can be seen that for cases in which Z_{eff}^{x} is used (for *Equation* 13), the error in the calculated ρ_e lies within 4% and can be as low as 0.8%. The error is large if the estimation is made using *Equation* (14) and ignoring the Z_{eff}^{x} to be close to that of water.

For Z_{eff}^{x} < 3500, *Equation* (14) gives ρ_e', which has an error that is less than 3%. In the case where 7000< Z_{eff}^{x} <32000, *Equation* (14) gives ρ_e' which has an error between *3-30%*, with an increase in errors as Z_{eff}^{x} increases. This implies that for substances whose Z_{eff}^{x} is known to be low (e.g. fat and soft tissues), *Equation* (14) can be utilized to find the electron density and be satisfied with an error that may be less than 4%. However, for substances with higher Z_{eff}^{x}(e.g., spongy bone), one has to

supply the $Z_{eff}{}^x$ value that is found independently and use *Equation* (13) to find the ρ_e value.

Table 3. Concentration (w/w %), electron density ($\rho_e \times 10^{23}$number of electrons per cm^3), $Z_{eff}{}^x$ of potassium hydroxide. *Equations* (13) and (14) are used to calculate electron density ρ_{e_cal} and ρ'_e. The data is taken from F (V=140) since the photoelectric effect is low in this case.

w/w%	$Z_{eff}{}^x$	ρ_e	ρ_{e_cal}	ρ'_e
5	7181	3.4259	3.4069	3.5553
10	11125	3.4482	3.4955	3.8018
15	15108	3.6438	3.5670	4.0384
20	19133	3.7133	3.6910	4.3452
25	23198	3.7203	3.7746	4.6148
30	27306	3.8497	3.8691	4.9080
35	31456	3.9839	3.9607	5.2079

Table 4. Concentration (w/w %), electron density ($\rho_e \times 10^{23}$number of electrons per cm^3), $Z_{eff}{}^x$ of glycerol. *Equations* (13) and (14) are used to calculate electron density ρ_{e_cal} and ρ'_e. The data is taken from F (140) since the photoelectric effect is low in this case.

w/w%	$Z_{eff}{}^x$	ρ_e	ρ_{e_cal}	ρ'_e
5	3236	3.3962	3.3672	3.3654
10	3194	3.4389	3.4021	3.3987
15	3153	3.4617	3.4404	3.4315
20	3111	3.4811	3.4854	3.4787
25	3069	3.5071	3.5137	3.5053
30	3028	3.5363	3.5454	3.5353
35	2986	3.5424	3.5906	3.5786
40	2944	3.6209	3.6558	3.6419

Table 5. Concentration (w/w %), electron density ($\rho_e \times 10^{23}$number of electrons per cm^3), $Z_{eff}{}^x$ of methanol. *Equations* (13) and (14) are used to calculate electron density ρ_{e_cal} and ρ'_e. The data is taken from F (140) since the photoelectric effect is low in this case.

w/w%	$Z_{eff}{}^x$	ρ_e	ρ_{e_cal}	ρ'_e
5	3225	3.2106	3.3076	3.3054
10	3173	3.1773	3.2828	3.2788
15	3122	3.1569	3.2613	3.2555
20	3070	3.1269	3.2398	3.2554
25	3019	3.0938	3.2116	3.2031
30	2967	3.057	3.1867	3.1754
35	2916	3.0335	3.1618	3.1488
40	2864	3.0063	3.1368	3.1221

Therefore, by using the least square values for V=140kVp (i.e., a (140)= 0.2891, b(140)= 3.355×10^{-6}), the predicted HU values for different substances are given in Table 6, in which $Z_{eff}{}^x$ = 3277 is used uniformly. This is a valid quantity for water and would not differ greatly for other substances, except for bones.

With the values of a(V) and b(V) being known, the HU (140) for water, adipose, breast, muscles, liver, as well as trabecular and spongy bones are calculated using *Equation* (13) by inserting the known ρ_e values. These ρ_e values were extracted from the technical manual of the CIRS model 062 electron density phantom It can be seen in Table 6 that these predicted values are very close to that which are generally observed, except for the bones as they have higher $Z_{eff}{}^x$ values than those for water. This implies that for substances with high $Z_{eff}{}^x$ values, their effective atomic numbers must be known independently for predicting the HU values.

From the known values of density, the predicted values of electron density from *Equation* 2 and HU (140) from *Equation* (8) for these objects are found to be close to values that are already reported in this study.

Table 6. Mass and electron density are shown by ρ (in gm/cm^3) and ρ_e (electron/ cm^3), respectively. Relative electron density (RED) relative to that of water, adipose, breast (50/50 adipose and fibro-glandular), muscle, liver, as well as trabecular and dense bones are denoted. Data are extracted from the technical manual of electron density reference phantom (CIRS model 062).

Tissue	ρ (gm/ cm^3)	$\rho_e \times 10^{23}$/cm^3	RED*	Predicted HU(140)
H$_2$O	1.00	3.34	1.00	00.44
Adipose	0.96	3.17	0.949	-51.60
Breast 50/50	0.99	3.261	0.976	-24.96
Muscle	1.06	3.483	1.043	41.41
Liver	1.07	3.516	1.052	51.28
Trabecular bone	1.161	3.730	1.117	115.27
Dense bone	1.61	5.512	1.512	648.08

*Relative Electron Density

The ρ values given in [17] were employed in Table 7. The calculated values of HU (120) for a Siemens SOMATOM plus 4 CT (Siemens Healthineers, Erlangen, Germany) were compared with those calculated by *Equation* (14) for different human tissues. It can be seen that the results predicted by the method in the present study are consistent with the findings given in the literature.

Discussion

According to the repeated results in this study, the mean HU value for water at the center of the axial slice of water was ΔHU_{water} = -3.2 regarding the acceptable range of -5<HU<5. Moreover, the image uniformity is acceptable since the deviations between HU values measured at different positions inside the axial slice is less than $\delta HU \leq \pm2$ HU everywhere, while the acceptable limit is ±4 HU on the basis of the IAEA No.19 [4].

Equation (11) (with F (V) ≈ 1.0) implies a deviation of -0.32% in the mean F (V) value of water, while the percentage error in F (V) at different positions is ±0.2%. The linear regression fit between X and Y has a high degree of goodness of fit with P<0.01. Furthermore, the accuracy of the calibration was tested by calculating the predicted ρ_e from *Equation* ((13) by using the regression coefficients a(V) and b(V).

These calculated values $\rho_{e(cal)}$ were compared with the actual values of ρ_e for all the samples prepared with KOH, glycerol, and methanol. The mean±SD of ratio:($\rho_{e\ (cal)}/\rho_e$) was 1.019±0.02 showing the accuracy of 2% of the prediction. This reliability is further tested by predicting the HU values of some known biological objects as is given in Table 6. These predicted HU values are seen to lie in the known range of HU for these substances. Large errors in the predicted ρ_e can take place if *Equation* (14) is used, and does not incorporate the role of $Z_{eff}{}^x$ which may be unknown.

Table 7. Comparison of the calculated HU results with those in [17].
The F (120) column shows the calculated values from the present study, and values given in [17] are displayed in $F_{Schn}(120)$ column.

Material	ρ(gm/cc)	$HU_{Schn}(120)$	HU(120)	$F_{Schn}(120)$	F(120)	$F(120)/F_{Schn}(120)$
Lung(blood filled)	0.26	-742	-740.9	0.259	0.259	1.000
Adipose3	0.93	-98	-73.34	0.902	0.926	1.026
Adipose2	0.95	-77	-53.42	0.923	0.946	1.025
Adipose1	0.97	-55	-27.77	0.945	0.966	1.022
Mammary gland1	0.99	-37	-13.56	0.963	0.986	1.024
Mammary gland2	1.02	-1	16.32	0.999	1.016	1.017
Brain cerebro spinal fluid	1.01	13	6.36	1.013	1.006	0.993
Adernal gland	1.03	14	26.29	1014	1.026	1.012
Small intestine (wall)	1.03	23	26.29	1.023	1.026	1.003
Urine	1.02	26	16.33	1.026	1.016	0.993
Gall bladder bile	1.03	27	26.29	1.027	1.026	0.999
Lymph	1.03	29	26.29	1.029	1.026	0.999
Pancreas	1.04	32	36.25	1.032	1.036	1.004
Prostate	1.04	34	36.25	1.034	1.036	1.002
Brain(white matter)	1.04	34	36.25	1.034	1.036	1.002
Testis	1.06	36	36.25	1.036	1.036	1.000
Brain(grey matter)	1.04	40	36.25	1.040	1.036	0.996
Muscle(skeletal)	1.05	40	46.22	1.040	1.046	1.005
Heart1	1.05	41	46.22	1.041	1.046	1.005
Kidney1	1.05	41	46.22	1.041	1.046	1.005
Thyroid	1.05	41	46.22	1.041	1.046	1.005
Aorta	1.05	42	46.22	1.042	1.046	1.004
Heart2	1.05	43	46.22	1.043	1.046	1.003
Kidney2	1.05	43	46.22	1.043	1.046	1.003
Liver1	1.05	43	46.22	1.043	1.046	1.003
Muscle(skeletal2)	1.05	43	46.22	1.043	1.046	1.003
Muscle(skeletal3)	1.05	43	46.22	1.043	1.046	1.003
Heart3	1.05	44	46.22	1.044	1.046	1.002
Mammary gland3	1.06	45	56.18	1.045	1.056	1.010
Kidney3	1.05	46	46.22	1.046	1.046	1.000
Ovary	1.05	46	46.22	1.046	1.046	1.000

The importance of knowledge of $Z_{eff}{}^x$ and its significance in accounting for photoelectric attenuation is dealt with in detail in the literature [13, 20-23]. In such cases, DECT measurements are to be made that can give both ρ_e and $Z_{eff}{}^x$ simultaneously.

The HU value increases linearly with increasing concentration of the chemical compounds with a physical density greater than water as in glycerol and KOH. The trend is linear; however, it is reverse for the chemical compounds with a physical density less than that of water as seen for methanol.

The linearity of the CT machine used in this study is found to be acceptable since it is able to produce the HU values that have a linear relationship with the concentration of simple chemical compounds, such as methanol, glycerol, and KOH. This also gives the proper trend for the slope.

For testing the performance of the CT machine, phantoms can be procured from the CT manufacturer or obtained from third-party suppliers. The HU values may be small for tissues with very low effective atomic number, such as alveolar tissues in the lung, and may have very large values for high atomic number tissues, including such bone tissues. The linearity measurement of the HU values is very important for proper reliability of the CT machines.

Kalender emphasized that linearity was required for CT systems, and it was already specified in the early days of CT [24-25] The practical problem noted decades ago in the past is still present with no provision of adequate test tools or correcting methods being at the disposal. The specification of a set of different plastics is inadequate, and the AAPM task group in its original specification acknowledged the "lack of rigor". The μ-values for plastics, such as polyethylene, Plexiglas, and Teflon depend on the spectrum and detector characteristics. Therefore, they will show different behavior for different scanners. Linearity can only be checked with the object and phantom inserts, in which only the mass density is varied; however, the composition and the energy-dependent mass-attenuation coefficient μ/ρ is kept constant.

As can be seen in Table 3, the preparations of such materials are indeed challenging, and the recorded μ-values for any substance would depend upon the particular CT's specifications, such as the source spectrum and detector efficiency which can widely vary [13]. However, artifacts due to non-linearity are reduced in homogeneous substances as is stated in [17] that the use of polychromatic X-ray sources in tomographic X-ray measurements leads to non-linear transmission effects.

Since these nonlinearities are not normally taken into account in tomographic reconstruction, the artifacts occur. These artifacts can be severe, especially when

imaging objects with multiple materials that contain widely varying X-ray attenuation coefficients.

To our knowledge, the need to test the linearity of CT system has not received adequate attention from researchers or equipment manufacturers, though its importance is considered even in textbooks on medical physics [10, 17, 26-28] and by several publications over several decades. Commercial manufacturers do not primarily focus on the question of linearity of CT machine. The usual tests by the commercially available phantoms, such as ACR phantom are done by the measurement of the HU values usually at 120 kVp of certain standard samples.

The HU values of these materials are measured by the CT machine and the measured HU values are compared with those suggested by the phantom manufacturer. The scientific basis for these suggestions are not disclosed but are treated as trade secrets or the manufacturer's "intellectual property". For instance, these kinds of tests do not directly suggest anything about the CT machine's linearity or how can one remove different artifacts. Furthermore, the HU values are machine dependent quantities. Therefore, a method was proposed in this study, which checks the linearity between HU and density (ρ) considering that this linear dependence may show different slopes for substances with different values of Z_{eff}.

This particular phantom has been constructed with the aim of aiding regular quality control of hospital equipment and for research on DECT inversion. Furthermore, the calibration materials are simple to prepare and have a close overlap of (ρ_e, Z_{eff}) with those of several biologically important substances. For instance, the electron density of low Z_{eff} materials, such as different concentrations of methanol are comparable to those of adipose and breast (50/50% adipose and fibro-glandular).

In the same line, chemical characteristics of medium Z_{eff} chemical compounds, such as glycerol are comparable to the values for muscle and liver in CIRS phantom inserts. Moreover, electron densities of high Z_{eff} chemical compounds, such as KOH are comparable to those of trabecular bone in the CIRS phantom, as can be seen in Tables 3 and 6.

Due to the high workload of CT systems, X-ray tubes are damaged frequently. Therefore, it needs to be replaced by a new X-ray tube every 6 to 12 months in a year, as experience shows. Before using each X-ray tube, the evaluation of the X-ray tube performance through quality control tests is necessary. In addition to the essential tests, such as the accuracy of HU values of water, noise measurement, and uniformity test, it is inevitable to evaluate the linearity of CT system and its ability to provide a wide range of HU values. Furthermore, liquid samples have been used for calibration because liquid solutions have high homogeneity. This was also suggested in the AAPM document earlier 24). Therefore, using the present method, the HU values are available for known

chemical compounds with high homogeneity, which can be developed as reference systems for linearity tests.

The CT phantom that is described in this study is easy to build and replicate. The methods that are followed to test the linearity of CT machines can be taken as standard procedures for linearity tests. The developed algorithm could be used to predict electron density and ultimately physical density of unknown tissues. Furthermore, limited financial resources of some of the medical imaging centers, especially those in developing countries may not allow them to purchase expensive phantoms that are manufactured by commercial medical physics companies. The design and production of simple and inexpensive phantoms, such as the type described in this study can help the physicist to check the essential equipment-parameters accurately, particularly those that are indispensable for quantitative studies, including testing the linearity of the CT system.

Such phantoms that are affordable to a larger number of medical scientists would prove to be of benefit for the progress of medical imaging science and also for health benefits to patients. The present equipment is seen to be a reliable device to determine the electron density of the scanned samples for low Z_{eff} materials, which are quite numerous in medical physics. Therefore, it serves as a very important tool in radiotherapy for dose calculation by treatment planning systems (24). In addition, this phantom can also be used for calibration of DECT equipment and the determination of both ρ_e and Z_{eff} as described in [29-31].

Conclusion

It was revealed in this study that an inexpensive and simple phantom designed and fabricated by the authors is free of extraneous effects. Moreover, it can be used to perform the essential quality control tests of the CT machine, such as the accuracy of HU value, noise measurement, image uniformity, the linearity of the CT machine, and the beam hardening effects. This phantom is able to predict the electron density of the scanned materials, and therefore to calibrate CT machines for the purpose of dose calculation in treatment planning for radiotherapy. In addition, this phantom can be used to detect the contribution from the photoelectric effect, thereby determining the value of, ρ_e. Accordingly, this phantom can be utilized for the calibration of DECT to quantitatively predict the chemical characteristic of ρ_e if the Z_{eff} value is low. This can be a useful method for the purpose of tissue characterization of the material under study. For complete characterization, one needs both ρ_e and Z_{eff}, which can be found only by the inversion of DECT data, a task that has to be developed with further studies.

Acknowledgment

References

1. Yoon YE, KooNon BK. Non-invasive functional assessment using computed tomography: when will they be ready for clinical use?. Cardiovasc Diagn Ther. 2012; 2: 106-12.
2. Mollet NR, Cademartiri F, Van Mieghem CAG, Runza G, McFadden EP, Baks T, et al. High-Resolution Spiral Computed Tomography Coronary Angiography in Patients Referred for Diagnostic Conventional Coronary Angiography. Circulation. 2005; 112: 2318-23.
3. Bazalova M, Carrier J-F, Beaulieu L, Verhagen F , Dual-energy CT-based material extraction for tissue segmentation in Monte Carlo dose calculations. Phys. Med.Biol. 2008 53: 2439-56.
4. Heismann B, Balda M, Quantitative image-based spectral reconstruction for computed tomography. Med. Phys. 2009 36: 4471-4485.
5. Govind AS, Sukumar S, Dkhar W, Grading of cerebral infraction using CT-Hounsfield unit to report the Hounsfield unit in acute, subacute and chronic stroke. International Journal of Current Research 2015 7:17874-78. Available from : http://www.journalcra.com
6. Cody DD, Pfeiffer D, McNitt-Gray MF, Ruckdeschel TG, Strauss KJ. Computed Tomography Quality Control Manual, American College of Radiology. available from: http://www.acr.org/~/media/ACR%20No%20Index/ Documents/QC%20Manual/2012CTQCManual1a Year: 2012.
7. International Atomic Energy Agency. HUMAN HEALTH SERIES NO.19 Quality. Assurance Program for Computed Tomography: Diagnostic and Therapy Applications. Austria Year: 2012.
8. AAPM Diagnostic X-Ray Committee. Specification and acceptance testing of computed tomography scanners. American Association of Physicists in Medicine; 1993.
9. Euclid S. Computed Tomography, physical principles, clinical applications, and quality control. Second edition, W.B. SAUNDERS COMPANY, A Harcourt Health Sciences Company, New York, United States of America. 2001.
10. Kalender WA. Computed Tomography, Fundamentals, System Technology, Image Quality, Publics Corporate Publishing.2005.
11. Cropp RJ, Seslija P, Tso D, Thakur Y. Scanner and kVp dependence of measured CT numbers in the ACR CT phantom. J Appl Clin Med Phys. 2013; 14: 338-49.
12. Akpochafor MO, Adeneye SO, Kehinde O, Omojola AD, Oluwafemi A, Nusirat A, et al. Development of Computed Tomography Head and Body Phantom for Organ Dosimetry. Iran J Med Phys. 2019; 16: 8-14.
13. Amini I, Akhlaghi P, Sarbakhsh P. Construction and verification of a physical chest phantom from suitable tissue equivalent materials for computed

14. Haghighi RR, Chatterjee S, Tabin M, Sharma S, Jagia P, Ray R, et al. DECT evaluation of non-calcified coronary artery plaque. Med Phys. 2015; 42: 5945-54.
15. Sunga R. Solutions for Technicians. Available from: http://www.handymath.com/mission.html .
16. Lide DR. CRC Handbook of Chemistry and Physics. CRC Press, New York. 1997.
17. Blumensath T, Boardman R.Non-convexly constrained image reconstructions from non-linear tomographic X-ray measurements. Phil. Transactions of the Royal Society A. 2015; 373. DOI:10.1098/esra.2014.0393.
18. Haghighi RR, Chatterjee S, Vyas A, Kumar P, Thulkar S. X-ray attenuation coefficient of mixtures: Inputs for dual-energy CT. Med Phys. 2011; 38:5270-9.
19. Haghighi RR. Evaluation of the coronary artery plaque. All India Institute of Medical Sciences. New Delhi, India. 2013.
20. Schneider W, Bortfeld T, Schlegel W. Correlation between CT numbers and tissue parameters needed for Monte Carlo simulations of clinical dose. Phys Med Biol. 2000; 45:459-78.
21. Schneider U, Pedroni E, Lomax A. The calibration of CT Hounsfield units for radiotherapy treatment planning. Phys Med Biol. 1996; 41 :111-24.
22. Shih CT, Wu J.Converting computed tomography images into photon interactions by using stoichiometric calibration and parametric fit models. Med Phys. 2017; 44:510-21.
23. Vanderstraeten B, Chin PW, Fix M, Leal A, Mora G, Reynaert N, Seco J, Soukup M, Spezi E, De Neve W, Thierens H. Conversion of CT numbers into tissue parameters for Monte Carlo dose calculations: a multi-centre study. Physics in Medicine & Biology. 2007 Jan 5;52(3):539.
24. Kalender WA, AAPM Report on Computed Tomograhy Scanners.. American Association of Physicists in Medicine; 1977
25. Pan X, Siewerdsen J, La Riviere PJ, Kalender WA, Radiation dose and image-quality assessment in Computed Tomography Radiology. Med Phys 2008 35:3728-39.
26. Judy PF. Phantoms for performance evaluation and quality assurance of CT scanners. American Association of Physicists in Medicine Report. 1977.
27. 27. Glover GH, Pelc NJ. Nonlinear partial volume artifacts in x- ray computed tomography. Medical physics. 1980;7(3):238-48..
28. 28. Park HS, Gao H, Lee SM, Seo JK. TOWARDS BEAM HARDENING CORRECTION FOR POLYCHROMATIC X-RAY CT. Journal of Computational Mathematics. 2016;34(6): 671-82.
29. Thomas SJ. Relative electron density calibration of CT scanners for radiotherapy treatment planning. Br J Radiol. 1999; 72: 781-6.
30. Thomas SJ. Relative electron density calibration of CT scanners for radiotherapy treatment planning. Br J Radiol. 1999; 72: 781-6.
31. Mandal SR, Bharati A, Haghighi RR, Arava S, Ray R, Jagia P, et al. Non-invasive characterization of coronary artery atherosclerotic plaque using dual energy CT: Explanation in ex-vivo samples. Phys Med. 2018; 45: 52-8.